

# Exploring a primordial solution for early black holes detected with the JWST

Pratika Dayal<sup>1</sup>

Kapteyn Astronomical Institute, University of Groningen, PO Box 800, 9700 AV Groningen, The Netherlands  
e-mail: p.dayal@rug.nl

July 16, 2024

## ABSTRACT

### Context.

*Aims.* With its rest-frame optical sensitivity, the James Webb Space Telescope (JWST) has unearthed black holes as massive as  $10^{6.2-8.1}M_{\odot}$  at redshifts of  $z \sim 8.5 - 10.6$ . In addition to these unexpectedly large masses, many systems show unexpectedly high black hole to stellar mass ratios of  $M_{\text{BH}}/M_{*} \gtrsim 30\%$  at these early epochs, posing a crucial challenge for theoretical models.

*Methods.* We start by collating data for all of the black holes confirmed with the JWST (through spectroscopy, X-rays or high-ionization emission lines). Using analytic calculations, we explore the combination of *astrophysical* seeding mechanisms and Eddington accretion rates that can explain the observed objects. We then appeal to *cosmological* primordial black hole (PBH) seeds and show how these present an alternative path for “seeding” early structures and their baryonic contents.

*Results.* Assuming seeding (via astrophysical means) at a redshift of  $z_{\text{seed}} = 25$  and continuous accretion, analytically all of the black holes studied here can either be explained through super-Eddington accretion (at an Eddington fraction of  $f_{\text{Edd}} \lesssim 2.1$ ) onto low-mass ( $100M_{\odot}$ ) seeds or Eddington-limited accretion onto high-mass ( $10^5M_{\odot}$ ) seeds. The upper limit, where we assume a primordial origin for all of these black holes, yields a continuous primordial black hole mass function (between  $10^{-5.25}$  and  $10^{3.75}M_{\odot}$ ) and a fractional PBH value  $\lesssim 10^{-12}$ , in good agreement with observational constraints. We then show how PBHs can seed a halo around themselves and assemble their baryonic (gas and stellar contents) starting at the redshift of matter-radiation equality ( $z \sim 3400$ ). We are able to reproduce the observed stellar and black hole masses for two of the highest redshift black holes (UHZ1 and GHZ9 at  $z \sim 10.3$ ) with the same parameters governing star formation, black hole accretion and their feedbacks. Exploring a wide swathe of model parameter space for GHZ9, we find black hole-to-stellar mass ratios ranging between 0.1 – 1.86 i.e. in some cases (of high supernova feedback), the black hole grows to be more massive than the stellar mass of its host halo, presenting an attractive alternative to seeding these puzzling early systems.

**Key words.** Galaxies: high-redshift – quasars: supermassive black holes – cosmology: theory – cosmology: early Universe – Black hole physics

## 1. Introduction

With its unparalleled sensitivity, the James Webb Space Telescope (JWST) has been crucial in shedding light on the black hole population in the first billion years of the Universe. These comprise both intrinsically faint (Harikane et al. 2023; Maiolino et al. 2023, 2024; Juodžbalis et al. 2024) and heavily reddened compact sources - the so-called “little red dots” (LRDs; e.g. Labbé et al. 2023a,b; Furtak et al. 2023, 2024; Kokorev et al. 2023; Matthee et al. 2023; Greene et al. 2024; Kokorev et al. 2024). These early observations have given rise to a number of tantalising issues such as: (i) clearly broadened Balmer lines have been used to infer black hole masses ranging between  $10^{7-8.6}M_{\odot}$  at redshifts  $z \sim 6-8.5$  (Kokorev et al. 2023; Harikane et al. 2023; Maiolino et al. 2023; Furtak et al. 2024; Juodžbalis et al. 2024; Greene et al. 2024). Additionally, high-ionization lines (Maiolino et al. 2024) and X-ray detections (Bogdán et al. 2024; Kovács et al. 2024) have been used to infer black hole masses as large as  $10^{6.2-7.9}M_{\odot}$  as early as  $z \sim 10.3 - 10.6$ . Such high masses pose a crucial challenge for theoretical models of black hole seeding and growth due to the lack of cosmic time available for their assembly (see reviews by e.g. Inayoshi et al. 2020; Fan et al. 2023); (ii) an over-abundance of black holes in the first billion years

(Harikane et al. 2023; Maiolino et al. 2023; Greene et al. 2024); and (iii) contrary to local relations that indicate black hole ( $M_{\text{BH}}$ ) to stellar mass ( $M_{*}$ ) ratios  $\lesssim 0.3\%$  for high-mass ellipticals (e.g. Volonteri & Reines 2016) or even lower than 0.01% (e.g. Suh et al. 2020), many of these early systems show unprecedentedly high ratios of  $M_{\text{BH}}/M_{*} \gtrsim 30\%$  (Kokorev et al. 2023; Juodžbalis et al. 2024; Bogdán et al. 2024; Kovács et al. 2024) which deviate from local relations at the  $> 3 - \sigma$  level (Pacucci et al. 2023). Interestingly, however, it has been shown that many of these black holes are compatible with local  $M_{\text{BH}}$ -velocity dispersion or  $M_{\text{BH}}$ -dynamical mass relations suggesting that while baryons might exist in the right amount in the host halos, they are inefficient at forming stars (e.g. Maiolino et al. 2023).

A number of works, however, urge caution in taking black hole and stellar masses at face-value. Drawing a parallel with Ultraluminous X-ray sources (ULXs), King (2024) warn that the emission from these sources could be beamed which would severely over-estimate the inferred luminosity. They also caution that standard virial indicators are unusable because the line velocity width broadening could be dominated by outflows in un-virialised broad line regions (BLRs). Using BLR models in different accretion regimes, Lupi et al. (2024) show that in many cases, super-Eddington accretion is preferred over the standard

Shakura & Sunyaev (Shakura & Sunyaev 1973) accretion disk, yielding black hole masses an order of magnitude lower than those inferred by applying “standard” local relations to single-epoch broad lines (from e.g. Greene & Ho 2007; Vestergaard & Osmer 2009; Reines & Volonteri 2015). Indeed, the offset of the inferred high-redshift  $M_{\text{BH}} - M_*$  relation from local ones could be explained by a combination of selection biases (such as finite detection limits and broad line detection requirements) and measurement uncertainties (Li et al. 2024) and only over-massive black holes being able to outshine their hosts making them “JWST-detectable” (Volonteri et al. 2023).

Observational issues notwithstanding, these puzzles have naturally prompted a flurry of research exploring the variety of black hole seeding and growth mechanisms allowed. In terms of *astrophysical* black hole seeds, “low-mass” seeds of mass  $\sim 10^2 M_\odot$  can be created by the collapse of metal-free (Population III; PopIII) stars in minihalos at high-redshifts (e.g. Carr et al. 1984; Abel et al. 2002; Bromm et al. 2002). “Intermediate-mass” seeds ( $\sim 10^3\text{--}4 M_\odot$ ) can form in dense, massive stellar clusters through a number of pathways (see e.g. Sec. 2.3.1 Amaro-Seoane et al. 2023) including dynamical interactions (e.g. Devecchi & Volonteri 2009), the runaway merger of stellar mass black holes (e.g. Belczynski et al. 2002) or the growth of stellar mass black holes in conjunction with mergers (e.g. Leigh et al. 2013; Alexander & Natarajan 2014). Finally, “heavy seeds”, the so-called direct collapse black holes (DCBHs;  $\sim 10^5 M_\odot$ ), can form via supermassive star formation (e.g. Loeb & Rasio 1994; Begelman et al. 2006; Habouzit et al. 2016), although this mechanism produces a lower number of viable seeds (Dayal et al. 2019). As of now, theoretical works allow a range of solutions for the existence of such massive black holes at early epochs including requiring heavy seeding mechanisms (Bogdán et al. 2024; Kovács et al. 2024; Maiolino et al. 2023; Natarajan et al. 2024), extremely efficient accretion and merger-driven growth of either light (Furtak et al. 2024) or intermediate mass seeds (Dayal et al. 2024), or heavy seeds which grow through mergers with light seeds and/or efficient accretion (Bhowmick et al. 2024). Heavy or intermediate-to-light mass seeds experiencing episodic super-Eddington accretion phases offer another option (Schneider et al. 2023; Maiolino et al. 2024), although the sustainability and effectiveness of super-Eddington accretion remains unclear (e.g. Regan et al. 2019; Massonneau et al. 2023). It has also been postulated that the dense and dust-rich environments of LRDs, in particular, could enable rapidly spinning black holes, maintained by prolonged mass accretion, that could result in over-massive black holes at these early epochs (Inayoshi & Ichikawa 2024). Theoretical analyses have also been used to demonstrate the need for both light and heavy seeding mechanisms (Fragione & Pacucci 2023) suggesting a continuum of seed masses rather than a bimodal distribution (Regan & Volonteri 2024).

However, *cosmology* provides an additional tantalising seeding mechanism in terms of “primordial black holes” (PBHs; Hawking 1971; Carr & Hawking 1974). We refer the reader to excellent reviews (e.g. Carr 2005; Carr & Green 2024) which detail how PBHs could be generated by a number of mechanisms including collapse from scale-invariant fluctuations (or cosmic strings), by cosmological phase transitions or by a temporary softening of the equation of state in the early Universe. We draw inspiration from a number of previous works which show how the Coulomb effect of a single black hole can generate an initial density fluctuation through the “seed” effect that can grow through gravitational instability to bind (dark matter) mass around itself - i.e. individual PBHs can essentially act as “seeds” of structure formation (Hoyle & Narlikar 1966; Ryan 1972; Carr & Rees

1984; Mack et al. 2007; Carr & Silk 2018; Carr & Kühnel 2020). Such PBHs have already been used to provide solutions for dwarf galaxy anomalies (Silk 2017), act as the seeds of high-redshift massive structures and massive black holes (Mack et al. 2007; Carr & Silk 2018) and to explain the excess seen in the cosmic X-ray background (Ziparo et al. 2022).

In this work, our aim is to study if PBHs assembling (isolated) halos around themselves offer a viable pathway for generating the massive black holes detected by the JWST. We start by collating data on all of the spectroscopically confirmed black holes detected by the JWST and their physical properties in Sec. 2. Assuming a seed redshift of  $z_{\text{seed}} = 25$  appropriate for *astrophysical* origins, we explore the seed masses (light/heavy) and growth (Eddington limited/super-Eddington accretion) mechanisms required to explain this data. For black holes inexplicable by different seed masses and Eddington-limited growth mechanisms, we appeal to *cosmology* and infer the PBH masses at the epoch of matter-radiation equality ( $z = 3400$ ) which are used to construct the PBH mass function; we ignore any growth of PBHs before this era since that is beyond the scope of this work. Finally, starting at  $z = 3400$ , we present an illustrative formalism of how such seeds could grow a halo around themselves, in addition to building their gas content and stellar components yielding values of  $M_{\text{BH}}/M_* \sim 0.1 - 1.86$ , in Sec. 3. We discuss the role of the model free parameters in Sec. 3.1 before concluding in Sec. 4.

We adopt a  $\Lambda$ CDM model with dark energy, dark matter and baryonic densities in units of the critical density as  $\Omega_\Lambda = 0.673$ ,  $\Omega_m = 0.315$  and  $\Omega_b = 0.049$ , respectively, a Hubble constant  $H_0 = 100 h \text{ km s}^{-1} \text{ Mpc}^{-1}$  with  $h = 0.673$ , spectral index  $n = 0.96$  and normalisation  $\sigma_8 = 0.81$  (Planck Collaboration et al. 2020). Throughout this work, we use a Salpeter initial mass function (IMF; Salpeter 1955) between  $0.1 - 100 M_\odot$  for the mass distribution of stars in a newly formed stellar population.

## 2. Inferring the primordial black hole mass function in light of JWST data

Analytically, the time evolution of the black hole mass,  $M_{\text{BH}}(t)$ , can be expressed as

$$M_{\text{BH}}(t) = M_{\text{seed}}(t_{\text{seed}}) e^{\left( \frac{4\pi G m_p f_{\text{Edd}}}{c \sigma_T} \frac{1-\epsilon}{\epsilon} (t - t_{\text{seed}}) \right)}. \quad (1)$$

Here,  $M_{\text{seed}}(t_{\text{seed}})$  is the seed mass at the starting time of  $t_{\text{seed}}$ ,  $f_{\text{Edd}}$  is the Eddington fraction,  $G$  is the universal gravitational constant,  $m_p$  is the proton mass,  $c$  is the speed of light,  $\sigma_T$  is the Thomson scattering cross-section and  $\epsilon$  is the radiative efficiency for which we use a value of 0.1 throughout the work. We explore the growth of black holes assuming seeding at a redshift of  $z_{\text{seed}} = 25$  (corresponding to  $\sim 134$  Myrs after the Big Bang), seed masses ranging between  $10^2\text{--}5 M_\odot$  and allowing both Eddington-limited and super-Eddington accretion. Allowing continuous accretion onto the black hole, this formalism implicitly assumes a maximal duty cycle of 100%.

We then collate data for all black holes confirmed by the JWST at  $z \gtrsim 4$ . As summarised in Table 1, there are a total of 34 such black holes identified through broad ( $\sim 1000\text{--}6000 \text{ km s}^{-1}$ ) Hydrogen balmer lines that are assumed to trace the kinematics of gas in broad-line regions (Kokorev et al. 2023; Kocovski et al. 2023; Harikane et al. 2023; Maiolino et al. 2023; Furtak et al. 2024; Greene et al. 2024), through high-ionization lines of Nitrogen and Neon (Maiolino et al. 2024) or through X-ray counterparts in deep *Chandra* observations (Bogdán et al. 2024;

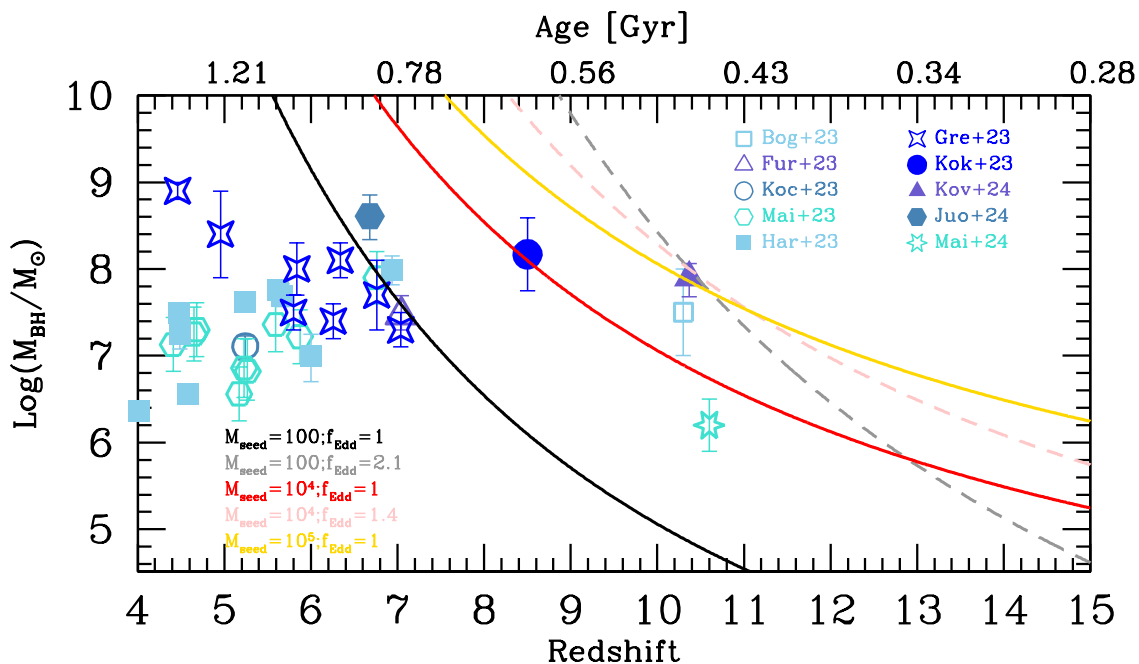


Fig. 1: The growth of black hole mass as a function of redshift (or cosmic time). Assuming seeding at a redshift of  $z_{\text{seed}} = 25$ , we show black hole growth considering both Eddington-limited ( $f_{\text{Edd}} = 1$ ) and super Eddington ( $f_{\text{Edd}} > 1$ ) accretion for seed masses of  $100$ ,  $10^4$  and  $10^5 M_{\odot}$ , as marked. As detailed in Table 1 and marked in the plot, we compare these models to black holes confirmed by: Bogdán et al. (2024), Furtak et al. (2024), Kocovski et al. (2023), Maiolino et al. (2023), Harikane et al. (2023), Greene et al. (2024), Kokorev et al. (2023), Kovács et al. (2024), Juodžbalis et al. (2024) and Maiolino et al. (2024).

Kovács et al. 2024). These have been used to infer the existence of massive black holes as large as  $10^{7.5} - 10^{8.1} M_{\odot}$  at  $z \gtrsim 8.5$ , only 600 million years after the Big Bang. A key caveat, however, is that these observations apply locally calibrated single-epoch relations to infer black hole masses from observed spectra/X-ray luminosities. This is driven by two key reasons: the first is that this provides a redshift-independent estimation of the black hole mass. The second is that local relations between line broadening (or X-ray emission) and the black hole mass are associated with small-scale (<pc scale) physics and dynamics which are not expected to show any significant dependence on the redshift (although see King 2024; Lupi et al. 2024).

As seen from Fig. 1, continuous Eddington-limited accretion onto low-mass ( $100 M_{\odot}$ ) seeds starting at  $z_{\text{seed}} = 25$  is able to yield black hole masses of  $M_{\text{BH}} \sim 10^{4.8} (10^{7.6}) M_{\odot}$  by  $z \sim 10.3$  (7). As a result, this model is able to explain 26 of the 34 JWST-observed black holes, leaving only 6 outliers. These comprise two of the  $z \sim 7$  massive black holes (Harikane et al. 2023; Juodžbalis et al. 2024) and all of the beasts observed at  $z \gtrsim 8.5$  (Kokorev et al. 2023; Bogdán et al. 2024; Kovács et al. 2024; Maiolino et al. 2024). Explaining these last 6 outliers with low-mass seeds requires invoking continuous super-Eddington accretion with  $f_{\text{Edd}} = 2.1$  that allows assembling  $M_{\text{BH}} \sim 10^8 M_{\odot}$  as early as  $z \sim 10.3$ .

Starting with a intermediate seed mass of  $10^4 M_{\odot}$  at  $z_{\text{seed}} = 25$  allows assembling a mass of  $M_{\text{BH}} \sim 10^{6.8} (10^{9.6}) M_{\odot}$  by  $z \sim 10.3$  (7), which encompasses *all* of the observed black holes apart from the two highest redshift objects at  $z \gtrsim 10$  (Bogdán et al. 2024; Kovács et al. 2024). Explaining these with such massive seeds requires invoking  $f_{\text{Edd}} = 1.4$ . Finally, already assembling a mass of  $M_{\text{BH}} \sim 10^{7.9} (10^{9.6}) M_{\odot}$  by  $z \sim 10.3$  (7), continuous Eddington accretion onto massive ( $10^5 M_{\odot}$ ) seeds is

able to explain all of the current observations, precluding the need for super-Eddington accretion.

To summarise, Eddington-limited accretion onto “low-mass” and “intermediate-mass” seeds result in 6 and 2 outliers (out of 34), respectively; seeds starting off as heavy as  $10^5 M_{\odot}$  at  $z = 25$  can explain all of the current data.

We then carry out a *Gedankenexperiment* where we assume a primordial origin for black holes and calculate the PBH mass assuming: (i): all of the black holes observed by JWST to have been seeded primordially - this yields the upper limit to the JWST-motivated PBH mass function; (ii): only the (6) BHs inexplicable by Eddington-accretion onto low-mass seeds are primordial; and (iii): only the (2) BHs inexplicable by Eddington-accretion onto intermediate-mass seeds are primordial. For each of these cases, we calculate the PBH seed mass ( $M_{\text{PBH}}$ ) reversing Eqn. 1 assuming a redshift of  $z = 3400$ ; we reasonably ignore any growth of PBHs before this era of matter-radiation equality. Calculating the PBH mass function also requires a number density associated with each seed - for this, we use the number densities quoted in the literature (see Table 1). These are usually obtained from the luminosity function (6th column). In the case of multiple objects contributing to a given luminosity function bin, we assign each of them the same weight in order to derive the number density per object (the 7th column) which are the values used here. The PBH mass function for each of these cases is shown in Fig. 2 with the PBH seed masses for each object noted in (column 9) of 1.

As seen, case (i) above yields an extended PBH mass function ranging between  $10^{-5.25} - 10^{3.75} M_{\odot}$ , reflecting the range of black hole masses and redshifts measured by the JWST. The mass function decreases by more than two orders of magnitude from a value of about  $10^{-3.1} \text{cMpc}^{-3}$  at  $M_{\text{PBH}} \sim 10^{-4.25} M_{\odot}$  to  $10^{-5.3} \text{cMpc}^{-3}$  at  $M_{\text{PBH}} \sim 10^{3.75} M_{\odot}$ . This reflects the few outliers in terms of mass and redshift as opposed to a large number

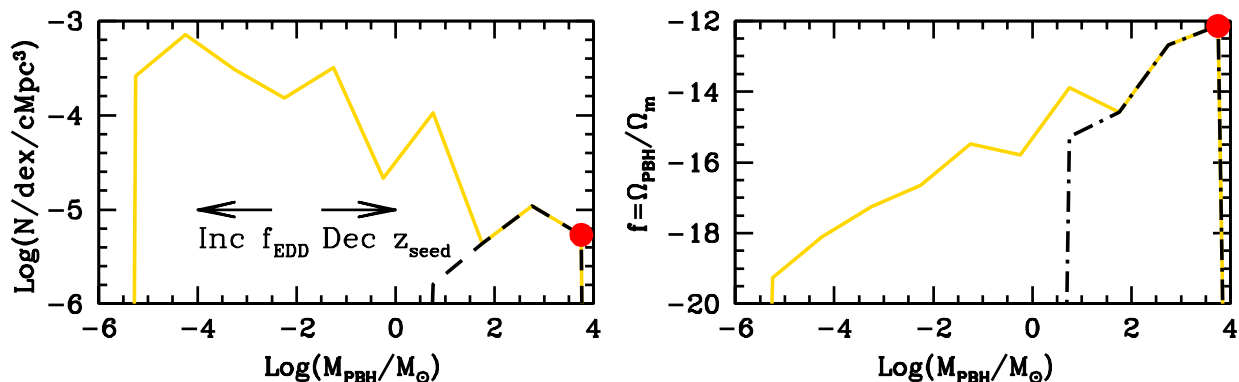


Fig. 2: As a function of the primordial black hole mass, we show the PBH mass function (*left panel*) and the fraction of dark matter composed of such objects (*right panel*). In both panels, these estimates are obtained assuming Eddington-limited accretion onto all black holes observed by the JWST (solid line; upper limit) and for those not explicable by Eddington-limited accretion on to low-mass seeds (dashed line) and intermediate mass seeds (point), respectively. As shown by arrows in the left panel, assuming super Eddington accretion would shift the mass function towards lower masses; on the other hand decreasing the seeding redshift would shift the mass function to higher masses.

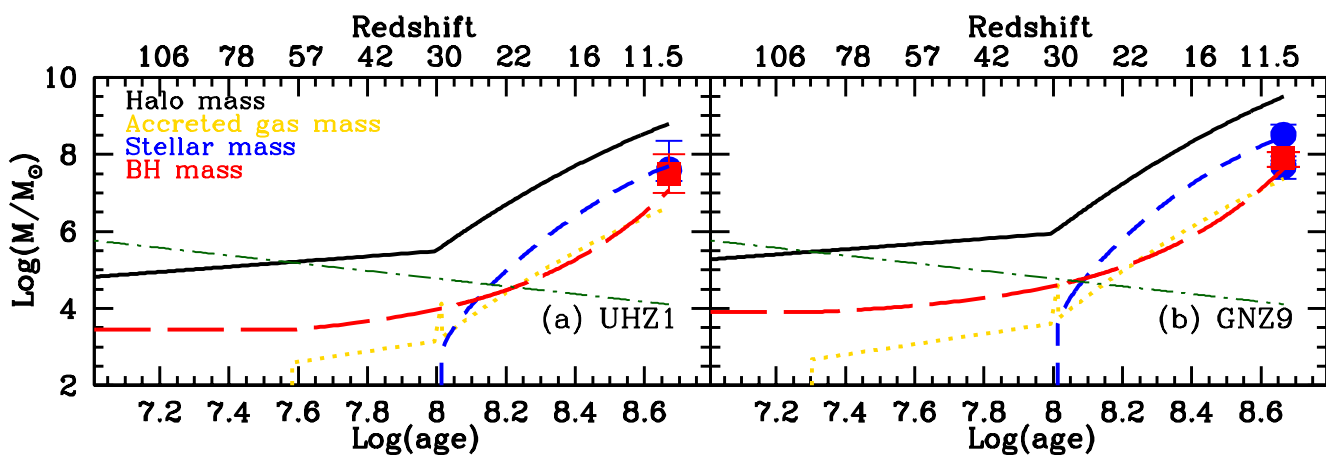


Fig. 3: The assembly of early galaxies in the scenario where primordial black holes act as the seeds of (isolated) structure formation. The left and right panels show the inferred stellar (blue points) and black hole (red points) masses for UHZ1 and GNZ9, observed at  $z \sim 10.3 - 10.4$ , respectively. As marked, we show the assembly of the black hole mass (long-dashed line), the halo mass (solid line), the accreted gas mass (dotted line) and the stellar mass (short-dashed line). In each panel, the dot-dashed line shows the evolution of the minimum halo mass that is able to bind halos with a baryonic over-density value of  $\delta_b = 200$ .

of “reasonable” mass black holes detected at  $z \lesssim 7$ . Indeed, the massive end of the PBH mass function (for  $M_{\text{PBH}} \gtrsim 10^{0.75} M_{\odot}$ ) is completely dominated by the outliers in case (ii) above, i.e., those lying above the Eddington accretion-limited mass onto low-mass seeds. Finally, given their similar masses and redshifts, the outliers in case (iii) above yield PBHs of very similar masses resulting in a single number density value of  $10^{-5.3} \text{cMpc}^{-3}$  at  $M_{\text{PBH}} \sim 10^{3.75} M_{\odot}$ . We note that assuming super Eddington accretion would shift the mass function towards lower masses; on the contrary, decreasing the seeding redshift would shift the mass function to higher masses.

We also calculate the density parameter for PBHs as a function of their mass and convert it to the usual notation of the fraction of dark matter in the form of PBHs as  $f = \Omega_{\text{PBH}}/\Omega_m$ . We show these results in (the right panel of) Fig. 2. We find that even in the “maximal” scenario where all JWST black holes are assumed to be primordial, the fractional PBH density parameter has a value  $\sim 10^{-19}$  for  $M_{\text{PBH}} \sim 10^{-5.25} M_{\odot}$  which increases to a maximum of  $\sim 10^{-12}$  for  $M_{\text{PBH}} \sim 10^{3.75} M_{\odot}$ . For this mass range, observational bounds mostly come from mi-

cro-lensing, gravitational waves, accretion and dynamical effects (Kavanagh 2024; Carr & Green 2024) and typically allow values of  $f \lesssim 10^{-2} - 10^{-3}$ . Being ten orders of magnitude lower, our results are in accord with current constraints and, as expected, show JWST-detected black holes to have a negligible contribution to the dark matter content.

### 3. Primordial black holes as seeds of early galaxy assembly

We now carry out illustrative calculations to show how the PBH masses calculated for the two outliers (UHZ1 and GNZ9) in case (iii) above (requiring super-Eddington accretion onto  $10^4 M_{\odot}$  seeds) could evolve into the systems observed by the JWST. In the “seed effect”, by a redshift  $z_h$  a PBH of mass  $M_{\text{PBH}}$  can bind a dark matter halo mass ( $M_h$ ) equal to (Carr & Silk 2018)

$$M_h = \frac{z_{mreq}}{z_h} M_{\text{PBH}}. \quad (2)$$

Here,  $z_{mreq} = 3400$  is the redshift of matter-radiation equality, which is when we assume the black hole can start assembling a halo around itself. In this formalism, by a redshift of  $z = 30$ , the halo mass is two orders of magnitude more massive than the black hole. Providing the dominant potential, at this point, we assume that the halo transitions to growing by smoothly accreting dark matter from the intergalactic medium (IGM). For this, we use results from high-resolution N-body (dark matter) simulations where the average halo accretion rate evolves with redshift as (Trac et al. 2015)

$$\langle \dot{M}_h \rangle = 0.21 \left( \frac{M_h}{10^8 M_\odot} \right)^{1.06} \left( \frac{1+z}{7} \right)^{2.5} \left[ \frac{M_\odot}{\text{yr}} \right] \quad (3)$$

We caution that this relation has been derived for halos ranging between  $10^{8-13} M_\odot$  at  $z \sim 6 - 10$ . However, we assume this relation holds out to  $z \sim 30$  given the lack of numerically-derived results at such early epochs and just use the average relation (without any scatter) for simplicity.

According to the spherical top-hat collapse model for halo formation, the virial temperatures of bound halos evolves as (Barkana & Loeb 2001)

$$T_{vir} = 1.98 \times 10^4 \left( \frac{\mu}{0.6} \right) \left( \frac{M_h}{10^8 h^{-1} M_\odot} \right)^{2/3} \left( \frac{\Omega_m \Delta_c}{\Omega_m^z 18\pi^2} \right) \left( \frac{1+z}{10} \right) \text{K}, \quad (4)$$

where we use a mean molecular weight value of  $\mu = 1.22$  appropriate for neutral primordial gas,  $\Delta_c = 18\pi^2 + 82d - 39d^2$  where  $d = \Omega_m^z - 1$ . Finally,  $\Omega_m^z = [\Omega_m(1+z)^3][\Omega_m(1+z)^3 + \Omega_\Lambda]^{-1}$ . At the high-redshifts ( $z \gtrsim 6$ ) considered in this work,  $\Omega_m^z \approx 1$  i.e.  $d = 0$  and  $\Delta_c = 18\pi^2$ . Next we model the response of baryons to dark matter potential wells (we refer the reader to Sec. 3.2 of the excellent review by Barkana & Loeb 2001). At  $z \lesssim 160$ , the gas temperature is decoupled from that of the cosmic microwave background (CMB) and evolves as  $\bar{T} \approx 170[(1+z)/100]^2 \text{K}$  (Barkana & Loeb 2001). Further, the over-density of baryons in a virialised object whose gravitational potential is driven by cold dark matter particles can be written as

$$\delta_b = \frac{\rho_b}{\bar{\rho}_b} - 1 = \left( 1 + \frac{6T_{vir}}{5\bar{T}} \right)^{3/2}, \quad (5)$$

where  $\rho_b$  is the gas density and the bar values denote background quantities. From Eqns. 4 and 5, we can calculate the minimum halo mass ( $M_h^{minb}$ ) that can host gas with a baryonic over-density of  $\delta_b = 200$  at any redshift. We caution this solution is approximate since it assumes gas to be stationary throughout the object and ignores entropy production in the virialization shock.

Once the assembling halo exceeds the  $M_h^{minb}$  value, we allow it to start building its gas content assuming that the assembling halo is able to drag in gas at a cosmological baryon-to-dark matter fraction i.e., the gas mass assembles at a rate of  $\dot{M}_g = (\Omega_b/\Omega_m)\dot{M}_h$ . We use a redshift step of  $\Delta z = 0.1$  to obtain the total halo and gas mass accreted in any given redshift step (or corresponding time-step). We allow the central black hole to grow by accreting a fraction of this gas

$$\Delta M_{BH} = \min[M_{Edd}, f_{BH} M_g^i]. \quad (6)$$

The black hole can therefore grow either by accreting the minimum between the Eddington mass and a fraction ( $f_{BH}$ ) of the available gas mass at the start of the redshift step ( $M_g^i$ ).

We finally allow star formation to take place at  $z = 30$ . The gas left over after black hole accretion is allowed to form stars with

an efficiency that is limited by feedback from TypeII Supernova (SNII; exploding stars more massive than  $8M_\odot$ ) such that (see Dayal et al. 2014; Mauerhofer & Dayal 2023)

$$\Delta M_* = (M_g^i - \Delta M_{BH}) f_*^{\text{eff}}, \quad (7)$$

where  $f_*^{\text{eff}} = \min[f_*^{\text{ej}}, f_*]$  is the ‘‘effective’’ star formation efficiency. Physically, this is the minimum between the star formation efficiency that produces enough SNII energy to ‘‘unbind’’ the remainder of the gas ( $f_*^{\text{ej}}$ ) and a maximum star formation efficiency parameter ( $f_*$ ). While  $f_*$  is a free parameter,  $f_*^{\text{ej}}$  can be calculated for any halo as

$$f_*^{\text{ej}} = \frac{v_c^2}{v_c^2 + f_*^w v_s^2}. \quad (8)$$

Here,  $v_c$  is the virial velocity of the host halo,  $f_*^w$  is the fraction of SNII energy that couples to the gas component and  $v_s^2 = \nu E_{51} = 61 \text{km s}^{-1}$ . Here,  $\nu = [134M_\odot]^{-1}$  is the number of SNII per stellar mass formed for our IMF and each SNII is assumed to impart an explosion energy of  $E_{51} = 10^{51} \text{erg}$ . We assume black hole and SNII feedback to act instantaneously on the gas component left after black hole accretion and star formation leaving a final gas mass at the end of a redshift step of

$$M_g^f = (M_g^i - \Delta M_{BH} - \Delta M_*) \left( 1 - \frac{E_{ej}}{E_{bin}} \right) \left( 1 - \frac{f_*^{\text{ej}}}{f_*^{\text{eff}}} \right), \quad (9)$$

where the second and third terms on the right hand side account for black hole and SNII feedback, respectively. Here,  $E_{ej} = f_{BH}^w \epsilon \Delta M_{BH} c^2$  is the ejection energy provided by the accreting black hole,  $E_{bin}$  is the binding energy of gas in the halo (for details see Dayal et al. 2019), and  $f_{BH}^w$  is the fraction of black hole energy that couples to gas. This ‘‘final’’ gas mass in a given redshift-step gets added to the accreted gas mass to form the new ‘‘initial’’ gas mass for the next redshift-step. Given that we assume black hole and SNII feedback to act instantaneously, the order of star formation or black hole accretion have no impact on the results.

The free parameters of the model (summarised in Table 2) are: the fraction of gas accreted onto the black hole ( $f_{BH}$ ), the threshold star formation efficiency ( $f_*$ ) and the fraction of black hole and SNII energies that couple to gas ( $f_{BH}^w$  and  $f_*^w$ ), respectively. In the interest of simplicity, in our *fiducial model*, we assume extremely weak feedback and use  $f_{BH}^w = f_*^w = 10^{-3}$ . We find black holes can always accrete at the Eddington rate rendering  $f_{BH}$  to be redundant parameter. We then find the value of  $f_*$  by matching to stellar mass measured for UHZ1 (Bogdan et al. 2024) using the PBH mass calculated in Sec. 2 and detailed in Table 1: we find a value of  $f_* = 0.7$  as shown in (the left panel of) Fig. 3. For this object, we start with a PBH seed mass of  $10^{3.4} M_\odot$  at  $z = 3400$  which initially binds the same mass in dark matter. By  $z = 30$ , the halo assembling around the black hole reaches a mass of  $M_h \sim 10^{5.5} M_\odot$ . It is only at  $z \sim 60$  that the halo is large enough to exceed  $M_h^{minb}$  and can start assembling its gas content. At this point, the black hole is allowed to start accreting and grows its mass by a factor 4 between  $z = 60$  and  $30$ . As a result, by  $z = 30$ , this halo has a black hole mass of  $M_{BH} = 10^4 M_\odot$ , a gas mass of  $M_g^i \sim 10^{4.1} M_\odot$  and  $M_* = 0$ . At  $z \lesssim 30$ , the halo transitions to smoothly-accreting dark matter from the IGM at a rate given by Eqn. 3 resulting in a halo mass of  $10^{8.8} M_\odot$  by the source redshift of 10.3. This is accompanied by smooth accretion of IGM gas which we (reasonably) assume to have a cosmological ratio of gas-to-dark matter. This results in

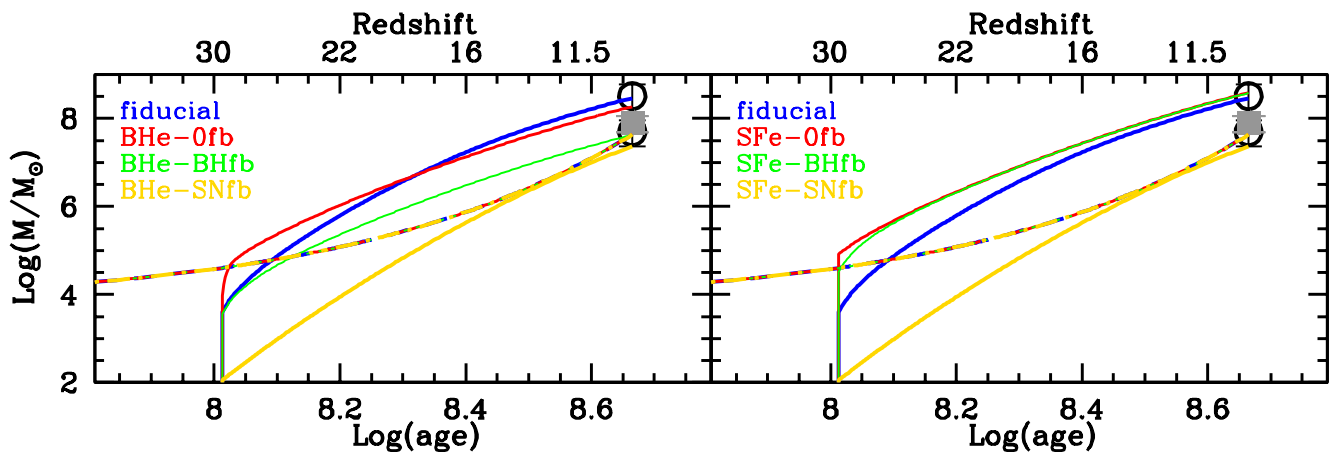


Fig. 4: The assembly of GHZ9 with primordial black holes acting as the seeds of structure formation. We show the assembly of the stellar mass (solid lines) and black hole mass (dashed lines) for 3 different models exploring the parameter space (see Table 2). While the *left* panel shows results for different feedback models in the case where black hole accretion is more efficient (BHe-) than star formation, the *right* panel shows results for the cases where star formation is allowed to be more efficient (SFe). The second part of the label in each panel shows the key feedback source - *0fb* stands for no feedback, *BHfb* for feedback from black holes alone and *SNfb* for SNI feedback alone.

the gas mass tracking the halo mass as shown in the same figure; we note that in this simplistic model of an isolated halo, accretion is the only mode through which the system can gain gas. In terms of the black hole mass, we find that it is able to grow efficiently at the Eddington rate. By  $z = 10.3$ , this black hole achieves a mass  $\sim 10^{7.1} M_{\odot}$ , comparable to the observationally inferred mass for UHZ1. Finally, given the low halo mass, star formation always proceeds at the ejection efficiency ( $f_*^{ej}$ ) such that at any time, the only gas mass available is that accreted in that time-step. Given the higher efficiency of the process, the stellar mass starts exceeding the black hole mass as early as  $z \sim 25.4$  and reaches a final value of  $M_* \sim 10^{7.7} M_{\odot}$  by the observed redshift. In this case, the final black hole to stellar mass ratio is about 0.25.

We then apply the same parameters to GHZ9 (right panel of Fig. 3) as a sanity check. This stellar mass of this object ranges between  $M_* = (4.9^{+2.0}_{-2.6}) \times 10^7 M_{\odot}$  (Atek et al. 2023) and  $M_* = (3.3^{+2.9}_{-2.4}) \times 10^8 M_{\odot}$  (Castellano et al. 2023). This object starts with a 2.8 times higher primordial black hole of mass  $10^{3.9} M_{\odot}$  - this allows its halo to exceed  $M_h^{minb}$  as early as  $z \sim 90$ . By the observed redshift of  $z = 10.4$ , this object has a halo mass of  $M_h \sim 10^{9.5} M_{\odot}$ . Additionally, without any change in parameters, we obtain final stellar and black hole mass values of  $10^{8.5}$  and  $10^{7.6} M_{\odot}$ , i.e.  $M_{BH}/M_* \sim 0.12$  in excellent accord with the observed values of the black hole mass (Kovács et al. 2024) and the stellar mass (as inferred by Castellano et al. 2023), as shown.

### 3.1. Impact of free parameters on model results

As detailed in Table 2, we now explore a wide range of models, including extreme combinations of the gas mass fractions available for black hole accretion/star formation and the fraction of black hole/SNII feedback coupling to the gas content. We apply these to GHZ9 to highlight the impact of parameter values on the stellar and black hole masses assembled. The results of these calculations are also shown in Fig. 4. We start by noting that the exact order of black hole accretion or star formation has no bearing on our results and that black holes always manage to accrete at the Eddington rate. As a result, the black hole assembly is the

same in every model, despite using values spanning the extrema of the parameter space.

We start by discussing the set of models where black holes are allowed to accrete the minimum between the Eddington mass and 90% of the available gas mass, with at most 10% of the gas forming stars, at any step. As shown in (the *left panel*) of Fig. 4), in the no feedback (BHe-0fb) model, the stellar mass reaches a final value of  $M_* \sim 10^{8.3} M_{\odot}$ , in agreement with the inferred value from Castellano et al. (2023) i.e.  $M_{BH}/M_* \sim 0.23$ . Including the impact of black hole feedback (BHe-BHfb) leads to a stellar mass that is almost 5 times smaller and has a value of  $M_* \sim 10^{7.6} M_{\odot}$  (in agreement with the mass estimate from Atek et al. 2023). Interestingly, in this case, the model yields a black hole mass that is larger than the stellar mass with a value of  $M_{BH}/M_* \sim 1.01$ . Finally, considering SNII feedback (BHe-SNfb) yields a very slow buildup of the stellar mass that reaches a final value of only  $M_* \sim 10^{7.4} M_{\odot}$ , again yielding a black hole mass that is larger than the stellar mass by a factor 1.86.

The case of efficient star formation, where the minimum between the ejection efficiency up to 90% of the gas is allowed to form stars, is shown in the *right panel* of the same figure. In this case, in the no feedback (SNe-0fb) and black hole feedback (SNe-BHfb) cases, the stellar mass is only 0.1 dex higher than that from the *fiducial* relation resulting in  $M_{BH}/M_* \sim 0.1$ ; these stellar masses are in accord with the higher mass estimates of Castellano et al. (2023). In the SNII feedback case (SNe-SNfb), a combination of high star formation rates and high feedback result in a final stellar mass of  $M_* \sim 10^{7.4} M_{\odot}$ , in accord with the values inferred by Atek et al. (2023), resulting in  $M_{BH}/M_* \sim 1.86$ .

To summarise, essentially all of the parameter space explored is compatible with the black hole and stellar masses inferred for GHZ9 given the wide range of  $M_*$  values observationally allowed for this object. Interestingly, the black hole-to-stellar mass ratios inferred from the different models explored range between 0.1 – 1.86 i.e. in some cases (high supernova feedback), the black hole actually manages to grow to be more massive than its host halo.

#### 4. Conclusions and discussion

The JWST has been instrumental in shedding light on black holes in the first billion years of the Universe. These unprecedented datasets have raised a number of tantalising issues including an over-abundance of black holes (Harikane et al. 2023; Maiolino et al. 2023; Greene et al. 2024), the presence of obese black holes ( $M_{\text{BH}} = 10^{6.2-8.1} M_{\odot}$ ) as early as  $z \sim 8.5 - 10.6$  (Kokorev et al. 2023; Maiolino et al. 2024; Bogdán et al. 2024; Kovács et al. 2024) and systems showing unprecedentedly high stellar-to-black hole mass ratios of  $M_{\text{BH}}/M_* \gtrsim 30\%$  (Kokorev et al. 2023; Juodžbalis et al. 2024; Bogdán et al. 2024; Kovács et al. 2024), compared to local relations where these values are two orders of magnitude lower (e.g. Volonteri & Reines 2016).

A number of works have cautioned the use of standard virial indicators in estimating black hole masses for such systems (King 2024) with others using BLR models to estimate black hole masses lower by an order of magnitude (Lupi et al. 2024). Finally, it has been noted that selection biases and measurement uncertainties could account for the offset of the inferred high-redshift  $M_{\text{BH}} - M_*$  relation (Li et al. 2024). These caveats notwithstanding, an enormous body of theoretical work has focused on *astrophysical* solutions including heavy seeding mechanisms (Bogdán et al. 2024; Kovács et al. 2024; Maiolino et al. 2023; Natarajan et al. 2024), episodic super-Eddington accretion phases (Schneider et al. 2023; Maiolino et al. 2024), extremely efficient accretion onto light or intermediate mass seeds (Furtak et al. 2024; Dayal et al. 2024) or heavy seeds which grow through mergers with light seeds and/or efficient accretion (Bhowmick et al. 2024).

In this work, we explore a complementary *cosmological* solution provided by *primordial black holes* (PBHs). These are seeded in the early Universe through mechanisms including collapse from scale-invariant fluctuations, cosmic strings, cosmological phase transitions or a temporary softening of the equation of state (see excellent reviews by e.g. Carr 2005; Carr & Green 2024). A key advantage of this scenario is that individual PBHs can act as “seeds” of structure formation, binding their dark matter halo around themselves (Hoyle & Narlikar 1966; Ryan 1972; Carr & Rees 1984; Mack et al. 2007; Carr & Silk 2018).

Starting by collating data on all of the 34 JWST-detected black holes confirmed at  $z \gtrsim 4$  (summarised in Table 1), we carry out analytic calculations to estimate the seed masses and accretion rates that would allow their assembly. We use these observations to derive limits on the PBH mass function. We then develop an illustrative model to show a PBH assembles its dark matter and baryonic content in the “seed” scenario. This is successfully applied to the highest-redshift outlying black holes observed (UHZ1, GHZ9). Our key findings are:

1. Starting at a redshift of  $z = 25$ , continuous Eddington-limited accretion onto low-mass ( $100 M_{\odot}$ ) seeds is able to explain 26 of the 34 JWST-observed black holes, leaving only 6 outliers (2 at  $z \sim 7$  and all of the 4 at  $z \gtrsim 8.5$ ). Explaining these requires invoking continuous super-Eddington accretion with  $f_{\text{Edd}} = 2.1$ . Eddington accretion onto intermediate-mass seeds ( $10^4 M_{\odot}$ ) explains 32 of the observed black holes apart from the two highest redshift objects at  $z \gtrsim 10$  (Bogdán et al. 2024; Kovács et al. 2024); explaining these requires invoking  $f_{\text{Edd}} = 1.4$ . Continuous Eddington accretion onto massive ( $10^9 M_{\odot}$ ) seeds is able to explain all of the current observations, precluding the need for super-Eddington accretion.
2. Assuming a PBH origin for *all* JWST black holes yields the upper limit to the PBH mass function. This shows an extended shape, with number densities  $\sim 10^{-3.1} \text{cMpc}^{-3}$  at

$M_{\text{PBH}} \sim 10^{-4.25} M_{\odot}$  to  $10^{-5.3} \text{cMpc}^{-3}$  at  $M_{\text{PBH}} \sim 10^{3.75} M_{\odot}$ . However, even in this “maximal” scenario, the fractional PBH density parameter has a maximum value  $\sim 10^{-12}$  which is ten orders of magnitude lower than current constraints - this implies PBHs from these JWST-detected early sources provide a negligible contribution to the dark matter content.

3. Considering PBHs to form the seeds of structure formation, we successfully show how the two highest redshift sources (UHZ1 at  $z \sim 10.3$  and GHZ9 at  $z \sim 10.4$ ) assemble their dark matter and baryonic contents with the same parameters governing star formation and black hole accretion and their associated feedbacks.
4. Exploring a wide swathe of parameter space in terms of black hole gas accretion, star formation efficiency and their associated feedbacks applied to GHZ9, we find black hole-to-stellar mass ratios between 0.1 – 1.86 i.e. in some cases (high supernova feedback), the black hole actually manages to grow to be more massive than its host halo.

We end with a few caveats: from the observational side, as noted, black hole masses are inferred using single epoch measurements calibrated against local relations. Further, the inferred stellar masses depend intricately on the assumed star formation history (SFH), stellar population properties (nebular emission inclusion, metallicity, dust attenuation) and, most crucially, the initial mass function - systematic uncertainties arising from these quantities can change stellar mass estimates by about an order of magnitude (Wang et al. 2024). Finally, we note that the black holes currently being observed only form a subset of the underlying population which might induce systematics in observed relations (e.g. Li et al. 2024).

In terms of the theoretical model, we have presented what is mostly an illustrative model of how a black hole can seed a halo and its baryonic components. We note that are a number of assumptions made that must be improved further: we transition from a linear (black-hole dominated) growth of the halo to non-linear when the halo becomes two orders of more magnitude than the black hole which must be investigated further. The accretion rates used here have also been derived for higher mass halos at lower-redshifts. Star formation and black hole accretion and their associated feedback could all be modelled in more detail. We also assume the black hole is able to remain stable at the centre of the halo and keep accreting with a duty cycle of a 100%.

In addition to the JWST, over the next decades, facilities such the Laser Space Interferometer Antenna (LISA) and Athena will be utterly crucial in understanding black holes and their hosts in the first billion years.

*Acknowledgements.* PD acknowledge support from the NWO grant 016.VIDI.189.162 (“ODIN”) and warmly thanks the European Commission’s and University of Groningen’s CO-FUND Rosalind Franklin program. PD thanks A. Mazumdar for illuminating discussions and L. Furtak, J. Greene and M. Mosbech for their comments that have added crucially to the quality of the work.

#### References

- Abel, T., Bryan, G. L., & Norman, M. L. 2002, *Science*, 295, 93  
 Alexander, T. & Natarajan, P. 2014, *Science*, 345, 1330  
 Amaro-Seoane, P., Andrews, J., Arca Sedda, M., et al. 2023, *Living Reviews in Relativity*, 26, 2  
 Atek, H., Chemerynska, I., Wang, B., et al. 2023, *MNRAS*, 524, 5486  
 Barkana, R. & Loeb, A. 2001, *Phys. Rept.*, 349, 125  
 Begelman, M. C., Volonteri, M., & Rees, M. J. 2006, *MNRAS*, 370, 289  
 Belczynski, K., Kalogera, V., & Bulik, T. 2002, *ApJ*, 572, 407  
 Bhowmick, A. K., Blecha, L., Torrey, P., et al. 2024, *MNRAS*, 531, 4311  
 Bogdán, Á., Goulding, A. D., Natarajan, P., et al. 2024, *Nature Astronomy*, 8, 126  
 Bromm, V., Coppi, P. S., & Larson, R. B. 2002, *ApJ*, 564, 23

No.	ID	Redshift	$\text{Log } \frac{M_{\text{BH}}}{M_{\odot}}$	Signature	$\text{Log } \frac{N_{\text{LF}}}{\text{cMpc}^3}$	$\text{Log } \frac{N_{\text{i}}}{\text{cMpc}^3}$	Reference	$\text{Log } \frac{M_{\text{PBH}}}{M_{\odot}}$
1	GHZ9	10.4	$7.9^{+0.16}_{-0.22}$	X-rays	-5.27	-5.57	Kovács et al. (2024)	3.9
2	UHZ1	10.3	$7.5^{+0.5}_{-0.5}$	X-rays	-5.27	-5.57	Bogdán et al. (2024)	3.4
3	Abell2744-QSO1	7.04	$7.47^{+0.22}_{-0.17}$	H $\beta$	-4.13	-4.44	Furtak et al. (2024)	0.7
4	CEERS 1670	5.24	$7.11^{+0.12}_{-0.16}$	H $\alpha$	-	-4.97	Kocevski et al. (2023)	-2.7
5	JADES1146115	6.68	$8.61^{+0.27}_{-0.24}$	H $\alpha$	-	-5.36	Juodžbalis et al. (2024)	2.3
6	GN-z11	10.6	$6.2^{+0.3}_{-0.3}$	N, Ne lines	-	-6.06	Maiolino et al. (2024), Fujimoto et al. (2023)	1.3
7	4286	5.84	$8.0 \pm 0.3$	H $\alpha$	-4.37	-4.97	Greene et al. (2024)	-0.6
8	13123	7.04	$7.3 \pm 0.2$	H $\alpha$	-4.58	-4.88	Greene et al. (2024)	0.5
9	13821	6.34	$8.1 \pm 0.2$	H $\alpha$	-4.37	-4.97	Greene et al. (2024)	0.4
10	20466	8.5	$8.14 \pm 0.42$	H $\alpha$	-4.88	-5	Greene et al. (2024), Kokorev et al. (2023)	2.9
11	23608	5.8	$7.5 \pm 0.2$	H $\alpha$	-5	-5	Greene et al. (2024)	-1.2
12	35488	6.26	$7.4 \pm 0.2$	H $\alpha$	-4.37	-4.97	Greene et al. (2024)	-0.5
13	38108	4.96	$8.4 \pm 0.5$	H $\alpha$	-4.37	-4.97	Greene et al. (2024)	-2.1
14	41255	6.76	$7.7 \pm 0.4$	H $\alpha$	-4.58	-4.88	Greene et al. (2024)	0.6
15	45924	4.46	$8.9 \pm 0.1$	H $\alpha$	-5	-5	Greene et al. (2024)	-3.1
16	CEERS01244	4.47	$7.5^{+0.04}_{-0.02}$	H $\alpha$	-3.04	-3.64	Harikane et al. (2023)	-4.5
17	GLASS 160133	4.01	$6.36^{+0.02}_{-0.01}$	H $\alpha$	-3.04	-3.64	Harikane et al. (2023)	-7.3
18	GLASS 150029	4.58	$6.56^{+0.03}_{-0.03}$	H $\alpha$	-3.04	-3.64	Harikane et al. (2023)	-5.1
19	CEERS 00746	5.62	$7.76^{+0.1}_{-0.1}$	H $\alpha$	-3.82	-4.12	Harikane et al. (2023)	-1.3
20	CEERS 01665	4.48	$7.27^{+0.16}_{-0.12}$	H $\alpha$	-5.05	-5.05	Harikane et al. (2023)	-4.7
21	CEERS 00672	5.66	$7.69^{+0.14}_{-0.12}$	H $\alpha$	-3.82	-4.12	Harikane et al. (2023)	-1.2
22	CEERS 02782	5.24	$7.62^{+0.11}_{-0.11}$	H $\alpha$	-3.85	-3.85	Harikane et al. (2023)	-2.2
23	CEERS 00397	6.0	$7.0^{+0.25}_{-0.11}$	H $\alpha$	-5.45	-5.45	Harikane et al. (2023)	-1.3
24	CEERS 00717	6.93	$7.99^{+0.16}_{-0.3}$	H $\alpha$	-5.79	-5.79	Harikane et al. (2023)	1.1
25	CEERS 01236	4.48	$7.25^{+0.2}_{-0.17}$	H $\alpha$	-3.04	-3.64	Harikane et al. (2023)	-4.7
26	8083	4.64	$7.25^{+0.31}_{-0.31}$	H $\alpha$	-3.06	-3.90	Maiolino et al. (2023)	-4.2
27	1093	5.59	$7.36^{+0.31}_{-0.31}$	H $\alpha$	-3.06	-3.90	Maiolino et al. (2023)	-1.7
28	3608	5.26	$6.82^{+0.38}_{-0.33}$	H $\alpha$	-3.83	-4.52	Maiolino et al. (2023)	-2.9
29	11836	4.40	$7.13^{+0.31}_{-0.31}$	H $\alpha$	-3.83	-4.52	Maiolino et al. (2023)	-5.1
30	20621	4.68	$7.3^{+0.31}_{-0.31}$	H $\alpha$	-3.06	-3.90	Maiolino et al. (2023)	-4.0
31	77652	5.23	$6.86^{+0.34}_{-0.34}$	H $\alpha$	-3.06	-3.90	Maiolino et al. (2023)	-3.0
32	61888	5.87	$7.22^{+0.31}_{-0.31}$	H $\alpha$	-3.83	-4.52	Maiolino et al. (2023)	-1.3
33	62309	5.17	$6.56^{+0.31}_{-0.31}$	H $\alpha$	-3.06	-3.90	Maiolino et al. (2023)	-3.4
34	954	6.76	$7.9^{+0.3}_{-0.3}$	H $\alpha$	-3.83	-4.52	Maiolino et al. (2023)	0.8

Table 1: A summary of the black holes confirmed by the JWST at  $z \gtrsim 4$ . For each object, we detail the ID (column 2), the redshift (column 3), the inferred black hole mass (column 4), the signature (column 5) and the number density from the luminosity function (column 6) as quoted by the cited work (column 8). We assign the same weight to each object in a given luminosity bin for a given work to infer the “individual” number density calculated in column 7. Finally, we quote the primordial black hole seed mass for each object assuming continuous Eddington-accretion onto this seed mass from a redshift of  $z = 3400$ .

No.	Model name	properties	$f_{\text{BH}}$	$f_*$	$f_{\text{BH}}^w$	$f_*^w$
1	fiducial	weak feedback	-	0.7	$10^{-3}$	$10^{-3}$
2	BHe-0fb	BH accretion efficiency > star formation efficiency, no feedback	0.9	0.1	0	0
3	BHe-BHfb	BH accretion efficiency > star formation efficiency, BH feedback only	0.9	0.1	0.1	0
4	BHe-SNfb	BH accretion efficiency > star formation efficiency, SN feedback only	0.9	0.1	0	0.1
5	SFe-0fb	star formation efficiency > BH accretion efficiency, no feedback	0.1	0.9	0	0
6	SFe-BHfb	star formation efficiency > BH accretion efficiency, BH feedback only	0.1	0.9	0.1	0
7	SFe-SNfb	star formation efficiency > BH accretion efficiency, SN feedback only	0.1	0.9	0	0.1

Table 2: The set of parameter values explored in this work. We explore a wide range of parameter space for the models noted in column 2 and their properties detailed in column 3. For each, we show the fraction of gas available for accretion onto the black hole (column 4), the maximum threshold efficiency for star formation (column 5) and the fractions of black hole and SNII feedback energies that can couple to gas (columns 6 and 7, respectively).



- Carr, B. & Kühnel, F. 2020, *Annual Review of Nuclear and Particle Science*, 70, 355
- Carr, B. & Silk, J. 2018, *MNRAS*, 478, 3756
- Carr, B. J. 2005, arXiv e-prints, astro
- Carr, B. J., Bond, J. R., & Arnett, W. D. 1984, *ApJ*, 277, 445
- Carr, B. J. & Green, A. M. 2024, arXiv e-prints, arXiv:2406.05736
- Carr, B. J. & Hawking, S. W. 1974, *MNRAS*, 168, 399
- Carr, B. J. & Rees, M. J. 1984, *MNRAS*, 206, 801
- Castellano, M., Fontana, A., Treu, T., et al. 2023, *ApJ*, 948, L14
- Dayal, P., Ferrara, A., Dunlop, J. S., & Pacucci, F. 2014, *MNRAS*, 445, 2545
- Dayal, P., Rossi, E. M., Shiralilou, B., et al. 2019, *MNRAS*, 486, 2336
- Dayal, P., Volonteri, M., Greene, J. E., et al. 2024, arXiv e-prints, arXiv:2401.11242
- Devecchi, B. & Volonteri, M. 2009, *ApJ*, 694, 302
- Fan, X., Bañados, E., & Simcoe, R. A. 2023, *ARA&A*, 61, 373
- Fragione, G. & Pacucci, F. 2023, *ApJ*, 958, L24
- Fujimoto, S., Wang, B., Weaver, J., et al. 2023, arXiv e-prints, arXiv:2308.11609
- Furtak, L. J., Labbé, I., Zitrin, A., et al. 2024, *Nature*, 628, 57
- Furtak, L. J., Zitrin, A., Plat, A., et al. 2023, *ApJ*, 952, 142
- Greene, J. E. & Ho, L. C. 2007, *ApJ*, 670, 92
- Greene, J. E., Labbe, I., Goulding, A. D., et al. 2024, *ApJ*, 964, 39
- Habouzit, M., Volonteri, M., Latif, M., Dubois, Y., & Peirani, S. 2016, *MNRAS*, 463, 529
- Harikane, Y., Zhang, Y., Nakajima, K., et al. 2023, *ApJ*, 959, 39
- Hawking, S. 1971, *MNRAS*, 152, 75
- Hoyle, F. & Narlikar, J. V. 1966, *Proceedings of the Royal Society of London Series A*, 290, 177
- Inayoshi, K. & Ichikawa, K. 2024, arXiv e-prints, arXiv:2402.14706
- Inayoshi, K., Visbal, E., & Haiman, Z. 2020, *ARA&A*, 58, 27
- Juodžbalis, I., Maiolino, R., Baker, W. M., et al. 2024, arXiv e-prints, arXiv:2403.03872
- Kavanagh, B. J. 2024, bradkav/NbodyIMRI: Release Version
- King, A. 2024, *MNRAS*, 531, 550
- Kocevski, D. D., Onoue, M., Inayoshi, K., et al. 2023, *ApJ*, 954, L4
- Kokorev, V., Caputi, K. I., Greene, J. E., et al. 2024, arXiv e-prints, arXiv:2401.09981
- Kokorev, V., Fujimoto, S., Labbe, I., et al. 2023, *ApJ*, 957, L7
- Kovács, O. E., Bogdán, Á., Natarajan, P., et al. 2024, *ApJ*, 965, L21
- Labbé, I., Greene, J. E., Bezanson, R., et al. 2023a, arXiv e-prints, arXiv:2306.07320
- Labbé, I., van Dokkum, P., Nelson, E., et al. 2023b, *Nature*, 616, 266
- Leigh, N. W. C., Böker, T., Maccarone, T. J., & Perets, H. B. 2013, *MNRAS*, 429, 2997
- Li, J., Silverman, J. D., Shen, Y., et al. 2024, arXiv e-prints, arXiv:2403.00074
- Loeb, A. & Rasio, F. A. 1994, *ApJ*, 432, 52
- Lupi, A., Trinca, A., Volonteri, M., Dotti, M., & Mazzucchelli, C. 2024, arXiv e-prints, arXiv:2406.17847
- Mack, K. J., Ostriker, J. P., & Ricotti, M. 2007, *ApJ*, 665, 1277
- Maiolino, R., Scholtz, J., Curtis-Lake, E., et al. 2023, arXiv e-prints, arXiv:2308.01230
- Maiolino, R., Scholtz, J., Witstok, J., et al. 2024, *Nature*, 627, 59
- Massonneau, W., Volonteri, M., Dubois, Y., & Beckmann, R. S. 2023, *A&A*, 670, A180
- Matthee, J., Naidu, R. P., Brammer, G., et al. 2023, arXiv e-prints, arXiv:2306.05448
- Mauerhofer, V. & Dayal, P. 2023, *MNRAS*, 526, 2196
- Natarajan, P., Pacucci, F., Ricarte, A., et al. 2024, *ApJ*, 960, L1
- Pacucci, F., Nguyen, B., Carniani, S., Maiolino, R., & Fan, X. 2023, *ApJ*, 957, L3
- Planck Collaboration, Aghanim, N., Akrami, Y., et al. 2020, *A&A*, 641, A6
- Regan, J. & Volonteri, M. 2024, arXiv e-prints, arXiv:2405.17975
- Regan, J. A., Downes, T. P., Volonteri, M., et al. 2019, *MNRAS*, 486, 3892
- Reines, A. E. & Volonteri, M. 2015, *ApJ*, 813, 82
- Ryan, Michael P., J. 1972, *ApJ*, 177, L79
- Salpeter, E. E. 1955, *ApJ*, 121, 161
- Schneider, R., Valiante, R., Trinca, A., et al. 2023, *MNRAS*, 526, 3250
- Shakura, N. I. & Sunyaev, R. A. 1973, *A&A*, 24, 337
- Silk, J. 2017, *ApJ*, 839, L13
- Suh, H., Civano, F., Trakhtenbrot, B., et al. 2020, *ApJ*, 889, 32
- Trac, H., Cen, R., & Mansfield, P. 2015, *ApJ*, 813, 54
- Vestergaard, M. & Osmer, P. S. 2009, *ApJ*, 699, 800
- Volonteri, M., Habouzit, M., & Colpi, M. 2023, *MNRAS*, 521, 241
- Volonteri, M. & Reines, A. E. 2016, *ApJ*, 820, L6
- Wang, B., Leja, J., Atek, H., et al. 2024, *ApJ*, 963, 74
- Ziparo, F., Gallerani, S., Ferrara, A., & Vito, F. 2022, *MNRAS*, 517, 1086